Electronic Supplementary Material (ESI) for Lab on a Chip.

Electronic Supplementary Information for **An *in vitro* tumor swamp model of heterogeneous cellular and chemotherapeutic landscapes**

Ke-Chih Lin[‡ab], Yusha Sun[‡a], Gonzalo Torga[c], Pema Sherpa[a], Yihua Zhao[d], Junle Qu[d], Sarah R. Amend[c], Kenneth J. Pienta[c], James C. Sturm[b], and Robert H. Austin[*a]

[a]Department of Physics, Princeton University, Princeton, NJ 08544, USA.
[b]Department of Electrical Engineering, Princeton University, Princeton, NJ 08544, USA.
[c]The Brady Urological Institute, Johns Hopkins School of Medicine, Baltimore, MD, 21287, USA.
[d]College of Physics and Optoelectronic Engineering, Key Laboratory of Optoelectronic Devices and Systems, Shenzhen University, Shenzhen, China.
[*]Corresponding author, e-mail: austin@princeton.edu.
[‡]These authors contributed equally.

Movies of long time-scale experiment: See Supplementary movies, including "control," "25 nM experiment 1," "15 nM experiment 1," and "15 nM experiment 2." The first and last in the list above were analyzed in the main paper for the length of 6 days. All movies incorporate the merged images of PC3-EPI (prostate cancer cell line) nuclei in green and a processed brightfield image in red that includes HS5 (bone marrow stromal cell line), with relevant gradients established from bottom (high-drug) to top (low-drug). Note that the brightfield images here also show, aside from stromal cells, PC3-EPI cytoplasm and background object outlines. The processing algorithms used for the processed brightfield images and green channel images are described in the below section. Movies are highly compressed in size for convenience and may lack detail. Higher-quality movies can be obtained from the authors.

Algorithmic design of image-processing protocols: Here, we briefly describe the particular protocols followed to obtain the quantifications in Fig. 8 (main text), Fig. 9 (main text), and Supplementary Fig. 3. For the analysis in Fig. 8 and Supplementary Fig. 3, we generated processed brightfield images as described in Supplementary Fig. 2 utilizing Fiji/ImageJ [1]. The red channel images that incorporated the cancer cell cytoplasmic regions were processed via Otsu's auto-thresholding algorithm locally [1]. The green channel images that portrayed the cancer cell nuclei were processed by a standard "adjust LUT" function within ImageJ and background subtraction [1]. To count the number of stromal cells, we proceeded as follows: *(1)* we first computed the percentage area covered inside each local microhabitat from the processed brightfield image; *(2)* we then found the percentage area covered by cancer cell cytoplasmic regions from the processed red channel image; *(3)* we subtracted the processed brightfield image from the processed red channel image to obtain the percentage area overcounted, as any portion of the red channel image that does not appear on the brightfield image must be due to extraneous fluorescence effects; *(4)* we then computed the percentage of the microhabitat covered by stromal cells only using

$$\%A \text{ stroma} = \%A \text{ brightfield} - \%A \text{ mCherry} + \%A \text{ overcounted}$$

where A signifies area and *(5)* we computed the number of stromal cells by dividing the area covered ($\%A\times$ area of microhabitat) by the average stromal cell size, which we estimated by manually running the above steps for several regions. The number of cancer cells were determined by the number of nuclei, which we counted within the processed green channel image by finding the number of maxima.

For the analysis in Fig. 9 to determine the average cell size, we employed the Analyze Particles function in ImageJ to the red channel images thresholded via the Default thesholding algorithm [1] to determine both the percentage area coverage and the number of cells in each microhabitat. We found that this method may slightly undercount the total number of cells when compared to the number estimated by counting the number of nuclei as described previously, mainly in areas of very high cell concentration. Thus, more advanced cell segmentation or machine learning algorithms may be employed to increase counting accuracy. Nevertheless, we note that this undercounting effect does not alter the illustration of the difference in cell size across the landscape, supporting our observations.

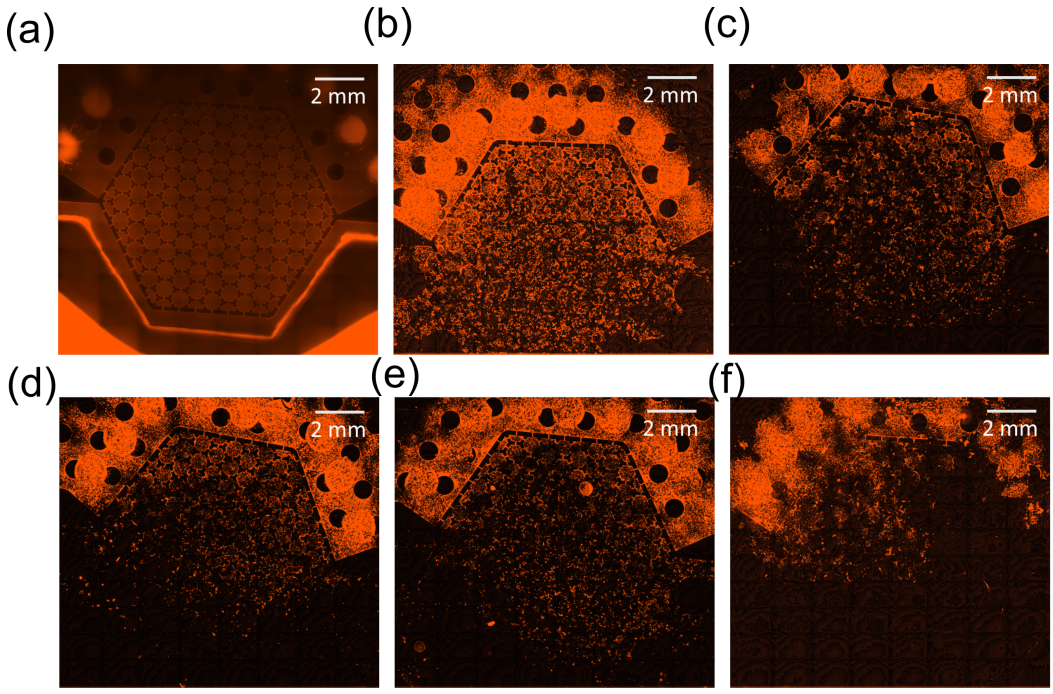

Figure 1: **Capacity for multiple simultaneous experimental conditions.** With the platform described in Fig. 3 in the main text, we illustrate the potential for parallel experimentation. In this instance, we show a representative visualization of a gradient test with Rhoadmine-6G (a), a control experiment (b), two 25 nM docetaxel gradient experiments (c–d), and two 15 nM docetaxel gradient experiments (e–f). For (b–f), PC3-EPI cell cytoplasm is shown in red.

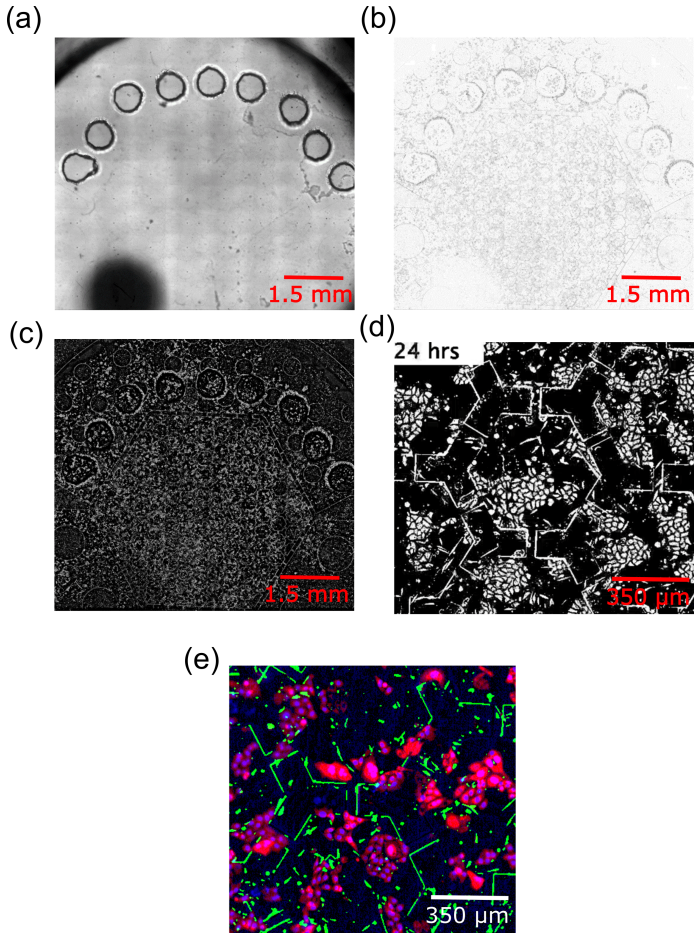

Figure 2: **Custom image-processing protocol for dual-labeled PC3-EPI prostate cancer cells and unlabeled HS5 stromal cells.** Note that the use of two fluorescent labels in one cell type limits the emission bandwidth for the rest of the cell types. Therefore, as a preliminary test, we used unlabeled HS5 and established a image processing protocol for brightfield image analysis and cell quantification. (a) Stitched mosaic of unprocessed 10X brightfield images. It is apparent that the background intensity differs dramatically across the field of view due to the flat-field effect, optical configuration, and most importantly unexpected objects that may scatter the transmission light source. (b) Correction for unevenly illuminated background via a rolling ball algorithm in ImageJ (background subtraction). Specifically, a local background signal is calculated by averaging over a large circle with assigned radius around the pixel. Sequentially, the calculated local background value is subtracted from original image to remove coarse background variations. (c) Further correction to determine local threshold value at each pixel to transform the background-subtracted image into a binary mask with cells illuminated. An adaptive local thresholding algorithm (Phansalkar) is employed via the Auto Local Threshold plug-in in Fiji [2]. The local thresholding scheme solves the problem of nonuniform brightfield intensity in our case. (d) A close-up image of part (c) reveals segmented cells. Typical image quantification methods can now be applied, including confluence, morphology (e.g. circularity, diameter), velocity, etc. (e) Overlay of cytoplasmic- and histone-labeled PC3-EPI and the processed brightfield channel at a location on a chip from (d) as an example. The green fluorescent protein histone label is pseudo-colored as blue. The mCherry cytoplasmic label is pseudo-colored as red. The mCherry image is subtracted from the processed brightfield image to generate a HS5-only image, pseudo-colored as green.

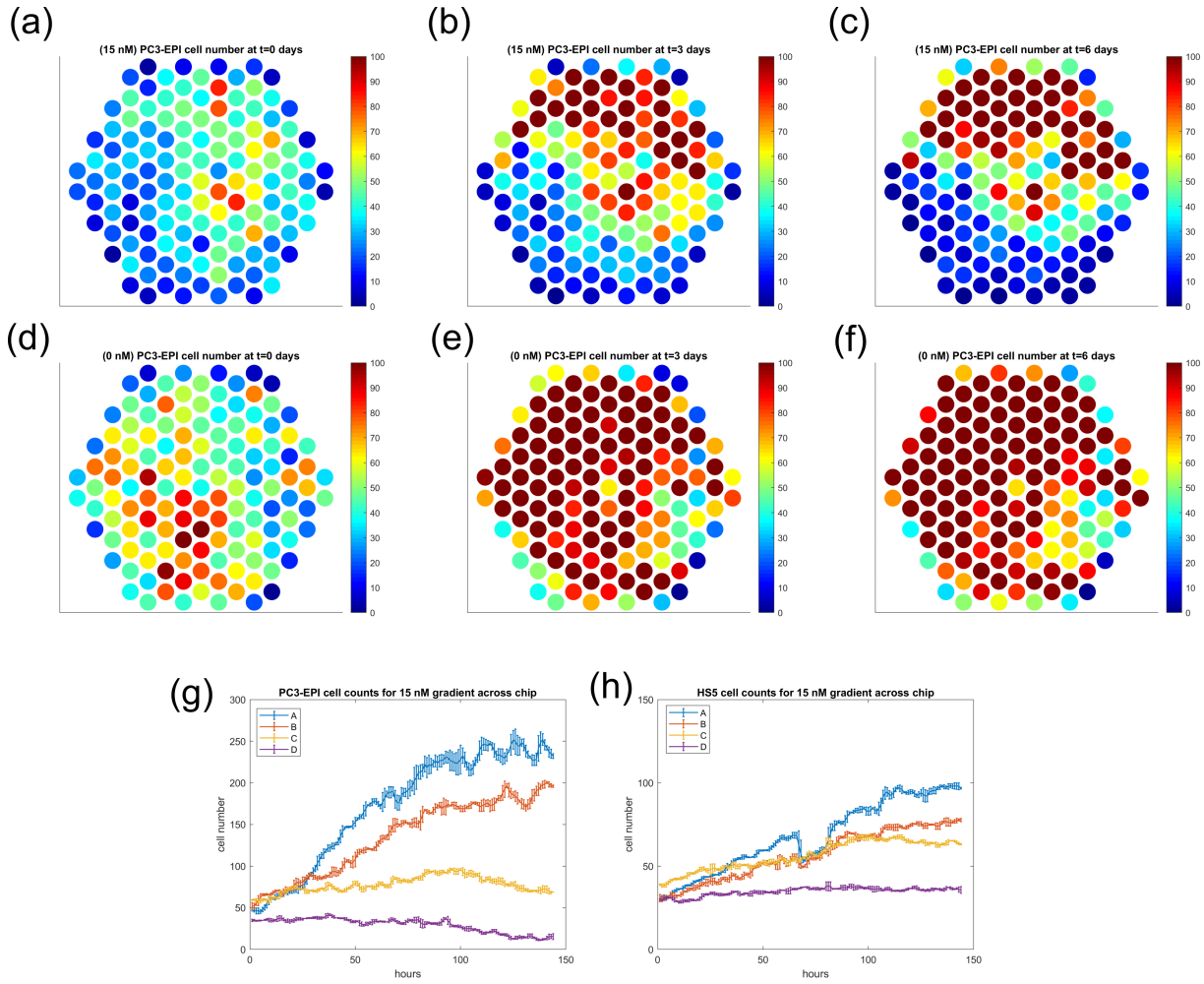

Figure 3: **Population spatial distribution of cancer PC3-EPI and stromal HS5 cells for gradient and control experiments.** (a) Analysis performed on images in Fig. 7d—f within the main text to determine the number of cancer cells in an experiment with 15 nM drug gradient at $t = 0$ days. The gradient is established from the bottom of the chip (high-drug area) to the top of the chip (low-drug area). Images are in heatmap form with cell number scale in a colorbar to the right of the spatial plot. (b) Similar plot as in (a) but for cancer cells at $t = 3$ days. (c) Similar plot as in (a) but for cancer cells at $t = 6$ days. (d—f) Analyses performed on images in Fig. 7a—c within the main text to determine the number of cancer cells at the relevant time points for the control (no drug gradient) experiment. (g) PC3-EPI cancer cell raw counts for regions A, B, C, D outlined in Fig. 8g in the main text over 6 days within the 15 nM drug gradient experiment. (f) Similar plot as in (g) but for stromal cell raw counts within the same experiment over 6 days.

References

[1] Schindelin, J., Arganda-Carreras, I., Frise, E., Kaynig, V., Longair, M., Pietzsch, T., ... & Tinevez, J. Y. (2012). Fiji: an open-source platform for biological-image analysis. Nature methods, 9(7), 676-682.

[2] Phansalkar, N., More, S., Sabale, A., & Joshi, M. (2011, February). Adaptive local thresholding for detection of nuclei in diversity stained cytology images. In 2011 International Conference on Communications and Signal Processing (pp. 218-220). IEEE.